IIM Metallurgy Materials Engineering   CrossMark

TECHNICAL PAPER

Evaluation of Mechanical Properties and Structure of Al-1100 Composite Reinforced with ZrO$_2$ Nanoparticles via Accumulative Roll-Bonding

Alireza Salimi[1] · Ehsan Borhani[1] · Esmaeil Emadoddin[1]

Abstract In this study, aluminum metal matrix composites reinforced with ZrO$_2$ nano-particles in volume fraction of 0.5, 0.75 and 1 % were manufactured through accumulative roll bonding (ARB) process. The results of composite microstructure indicated excellent ZrO$_2$ particle distribution in the Al matrix after 10 cycles of ARB process. The X-ray diffraction results also showed that nanostructured Al/ZrO$_2$ nano-particles composite with the average crystallite size of 48.6 nm was successfully achieved after 10 cycles of ARB process. The tensile tests were conducted on the ARBed strips. The tensile strength increased 2.15 times more than the initial value. The elongation dropped abruptly at the first cycle, and then increased slightly. The SEM images observations from the fracture surface showed that after 10 cycles of ARB process the fracture was almost shear fracture mode with fine and stretched pores.

Keywords Accumulatively roll-bonded · Composites · Microstructure · ZrO$_2$ · Nanoparticles

1 Introduction

Severe plastic deformation (SPD) is considered as an effective method in the production of bulk ultra-fine grained (submicron-grain sized 100 nm < d < 1 μm) or nanostructure ($\sim$<100 nm) metals [1, 2]. To date, SPD techniques such as, equal channel angular pressing (ECAP) [3], high pressure torsion (HPT) [4], torsion straining (TS) [5], cyclic

extrusion compression (CEC) [6] and accumulative roll bounding (ARB) have been developed [7–14]. The ARB process is one of the SPD methods proposed by Saito et al. [1] to achieve ultra-high strain in metallic materials without changing the specimen dimension. The roll bonding technique has been extensively used to fabricate metal matrix composite (MMC) because of its cost effectiveness and efficiency. The addition of ceramic reinforcements such as carbides and oxides to form MMCs enhances the properties such as elastic modulus, strength, wear resistance, and high-temperature durability [15]. MMCs are broadly used in components of various pieces of industrial equipment [16]. According to the fast developments in electronic industries, there is a great, unprecedented demand for high-strength, high conductivity materials [17]. At present, many types of composites are fabricated via roll bonding, including Al/SiC [18], Al/Al$_2$O$_3$ [19], Al/B$_4$C [20], Al/TiO$_2$ [21], Al/W$_P$ [22] and Al/CNT [23]. On the other hand, Zirconium oxide (ZrO$_2$) has attracted considerable attention because of its diverse practical applications in fuel-cell technology, as a catalyst or catalyst support, oxygen sensor, nanoelectronic devices, thermal–barrier coating, ceramic biomaterial. The ZrO$_2$ nano particles are currently of significant interest in preparing piezoelectric, electro optic, dielectric, and nanocomposite materials [24, 25]. The aim of this study is to produce the high-strength and highly-uniform metal matrix composites reinforced with different content of ZrO$_2$ nanoparticles (Al/ZrO$_2$) by the ARB process.

2 Experimental Procedures

The commercial pure aluminum sheet was used as matrix in this study. The chemical composition and some mechanical properties of this sheet are shown in Table 1.

✉ Ehsan Borhani
  e.borhani@semnan.ac.ir

[1] Faculty of Materials and Metallurgical Engineering, Semnan University, Semnan, Iran

🙋 Springer

Table 1 The chemical composition and mechanical properties of the Al matrix

Materials	Chemical composition	Sheet dimensions (l.w.t) (mm × mm × mm)	Elongation (%)	Yield strength	Crystallite size
Commercial Al sheet	0.18Si, 0.37Fe, 0.13Cu, 0.02Mn, 99.28Al, 0.02 others	120 × 50 × 1	43	89 MPa	43 μm

This sheet was cut into 120 mm × 50 mm × 1 mm pieces, parallel to the sheet rolling direction. These strips were annealed at 753 K in ambient atmosphere for 120 min.

The nanoparticles with particle volume fraction of 0.50, 0.75 and 1.0 % was used as reinforcement. The ARB process was used in order to produce Al-ZrO$_2$ composite. The ARB experiments were carried out with no lubrication, using a rolling mill, with a loading capacity of 20 tons. The microstructures of the sheets characterized by a scanning electron microscope with a field emission type gun (FE-SEM; Philips XL30) operated at 15 kV. The tensile test of the specimens after ARB process was conducted according to the ASTM E8M standard, prepared along the rolling direction. The gauge width and length of the tensile test samples were 6 and 25 mm, respectively. The tensile tests performed at room temperature at an initial strain rate of 8.3×10^{-4} s^{-1}. The total elongation of the samples was determined as the difference between gauge lengths before and after testing. In order to evaluate the hardness and assess microhardness changes, at different cycles of the ARB process, the X-ray pattern of the manufactured Al/ZrO$_2$ nanocomposite was recorded with an X-ray diffractometer (XRD).

3 Results and Discussion

3.1 Microstructure

Figure 1 shows the SEM image of the ZrO$_2$ Nano-particles used as reinforcement, having mean particle size of 60 nm, as indicated in Fig. 1b, and a purity of 99.9 %. The Al matrix composite fabricated by the ARB process uses 0.5, 0.75 and 1.0 vol% of ZrO$_2$ nano particles as reinforcement. Figure 2 shows SEM micrograph of the composite structure produced with 1.0 vol% at various ARB cycles. Distribution of ZrO$_2$ reinforcement particles in the aluminum matrix is obvious in different cycles (5 and 10 cycles). Figure 2a shows the 5 cycles ARB processed specimen in which a number of layers of reinforcing particles (indicated by arrows) can be seen within the matrix as continuous lines [26]. As the ARB cycle increases, the number of layers gradually increases, leading to more distribution of ZrO$_2$ reinforcement particles in the aluminum matrix. Distribution of reinforcement particles is important since they are very effective in improving the properties of composites [19, 20]. Reinforcement particles

play an important role in strain hardening and microstructure grain refinement and can be effective in modifying the microstructure in different ways including (a) barriers to dislocation motion, (b) differences in coefficient of thermal expansion between matrix and reinforcement particles and (c) increased dislocations by Orowan mechanism based on which ceramic particles act as an obstacle in the path of dislocation motion and by passing dislocation around the particle, Orowan loop is formed and the strength is increased [27–29].

According to the film theory, it can be said that two sheets of surface oxide layers develop cracks during rolling, and by rolling vertical force, new matrix materials are extruded through the cracks [21]. Now it can be said that in the presence of ZrO$_2$ particles between sheets of aluminum, particles in matrix can be extruded through the clusters. Figure 2a indicates areas, marked by circles, as the matrix extrudes among the reinforcement particle clusters. On the other hand, areas with square lines display ZrO$_2$ reinforcement particles aggregation in the form of agglomeration and cluster. Figure 2b displays higher magnification image of the composite structure. In this figure, the particle-free areas (circles) are shown together with cluster areas and reinforcement particle agglomeration which are marked with square lines. During the ARB process, elongation is caused in the rolling direction because of the reduced sectional area. This phenomenon causes the clusters being drawn in the rolling direction and the expansion thus created helps to break down the clusters resulting in gradual removal of clusters and areas devoid of reinforcement particles for a homogeneous structure to be created. In other words, separation and fracture of ZrO$_2$ nanoparticle increase during rolling process, as in each rolling stage the length of sample increases twice, due to 50 % thickness reduction. Optimizing the properties of the composite particularly achieves suitable combination of high strength and ductility which requires a relatively high volume fraction and fine reinforcement particles. On the other hands, it has been already reported [18] that, larger reinforcement particles have more uniform distribution than the smaller reinforcement particles, the composite with smaller reinforcement particles will have higher strength though. It can also be stated that with increasing the number of cycles, reinforcement particle distribution in the matrix improves and the distance between reinforcement particles increases, leading to the increase in strength. The nano sized and fine reinforcement particles tend to
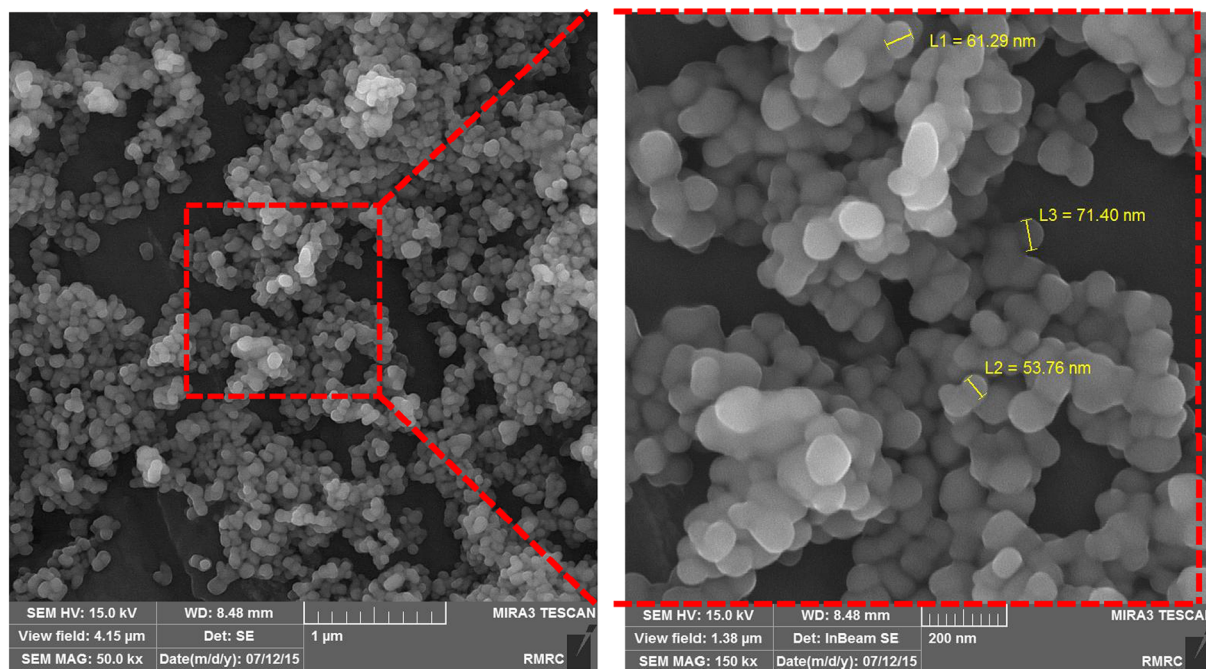
Fig. 1 The SEM micrograph of **a** ZrO$_2$ nanoparticles powder and **b** high magnification of selected area in **a**

non-uniform distribution and the creation of clusters and their agglomeration [18]. There is a direct relationship between the local volume fraction of reinforcement particles and the formation of defects that causes damage. Under external load, concentrated clusters of reinforcement particles may bring about non-uniform stress distribution in the produced composite. Significant three-dimensional stress is created in areas of clusters which are much larger than the applied stress, leading to faster formation and propagation of cracks [21]. The flow of plastic material in the center of clusters of particles is suspended because of high hydrostatic stresses causing cracks to germinate in these areas [20–23, 27]. Therefore reinforcement particle distribution in the matrix is very important. Figure 2c shows the image of the 10 cycles ARB processed composite structure. As shown in this figure, a structure with almost uniform ZrO$_2$ reinforcement particle distribution in aluminum matrix is achieved. According to Eq. (1) and the XRD result, the average crystallite size of 10 cycles ARB processed specimens with particle volume fraction of 0.5, 0.75 and 1 vol% are 85.5, 55.7 and 48.6 nm, respectively.

The crystallite size of the specimen calculated from the XRD patterns applying the Williamson–Hall method [30, 31].

$$\beta cos\theta = \frac{k\lambda}{d} + 2A\varepsilon sin\theta \qquad (1)$$

where θ is the Bragg diffraction angle, d is the crystallite size, ε is the average internal strain, λ is the wavelength of X-ray (0.154056 nm for Cu Kα radiation), β is the diffraction peak width at half maximum intensity, k is the Sherrer constant (0.91), and A is a coefficient, depending on the distribution of strain, which is near to unity for dislocations.

4 Mechanical Properties

### 4.1 Tensile Strength and Elongation

Engineering stress–strain curves of annealed aluminum and nanocomposites with different ZrO$_2$ contents are shown in Fig. 3. Also, Fig. 4 shows the variations of the tensile strength of nanocomposites versus the number of ARB cycles. As can be seen in Fig. 4, it is obvious that with increasing the number of cycles, the tensile strength improves for all nanocomposite samples. The tensile strength of composites with 0.5, 0.75, and 1.0 vol% ZrO$_2$ improves from 89 (for the annealed sample) to 121.5, 119, and 115 MPa after the first cycle, registering 37, 34, and 29 % increase, respectively. The tensile strength improves continually until the tensile strength of the ARB-processed composites with 0.5, 0.75, and 1.0 vol% ZrO$_2$ after the tenth cycle is about 1.85 times (164 MPa), 2.1 times (187 MPa), and 2.15 times (191.5 MPa) higher than that of the annealed sample. As it is clear, the tensile strength shows a higher rate of increase in the primary cycles and a lower rate of increase in the last cycles. Certainly, increased strength at the first cycles is due to work hardening (dislocation strengthening) [32]. In other words,
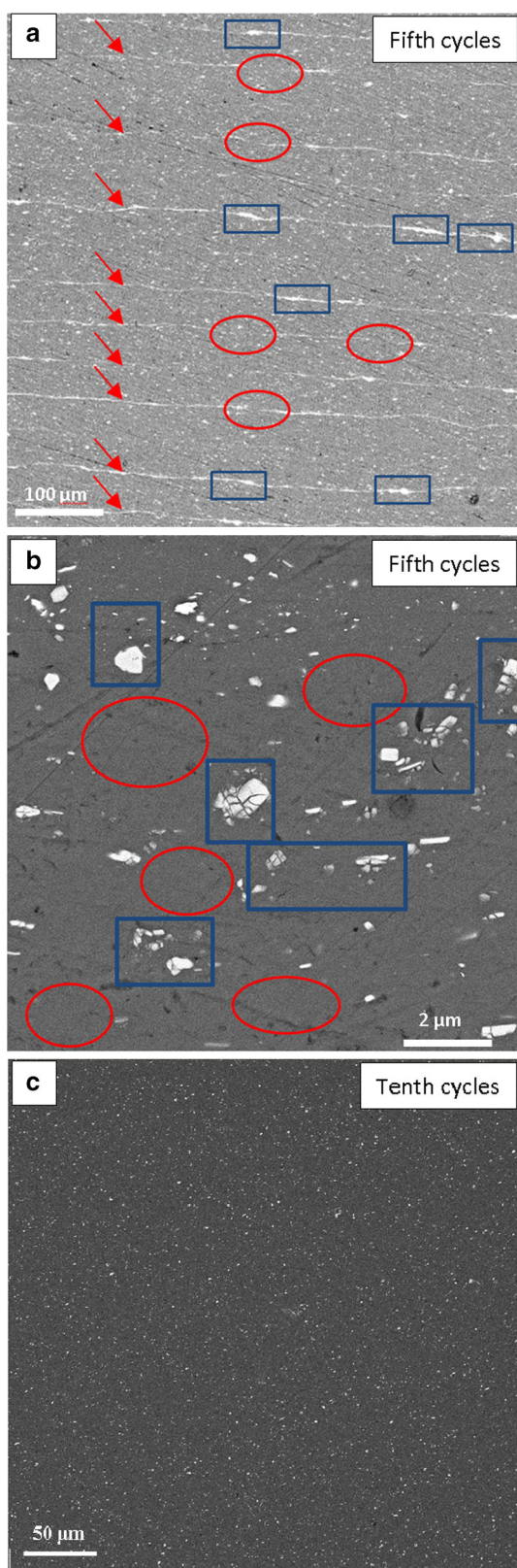
Fig. 2 The SEM micrograph of nanocomposite during ARB, **a** the reinforcing particles by a certain mechanism out of cluster state at cycle 5, **b** some areas of agglomerated reinforcing particles and areas free of particles and particle clusters at cycle 5, **c** the structure of nanocomposites reinforced with particles of ZrO_2 at cycle 10
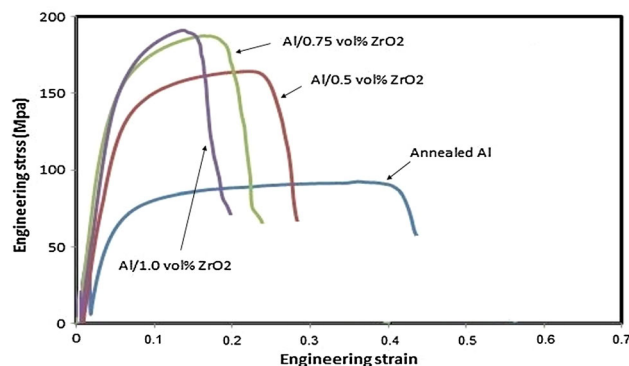
Fig. 3 Engineering stress–strain curves of the annealed and the ARB processed nanocomposites samples
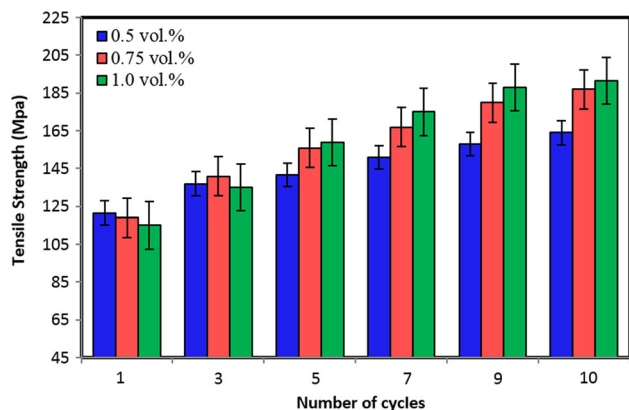
Fig. 4 Image of tensile strength-the number of cycles for produced composites by ARB process

However, in higher cycles, increased strength is due to the formation of ultra-fine grains (grain boundary strengthening mechanism) and evolution of granular structure (Hall–Petch effect) [33]. In this state, the effect of work hardening gradually decreases, as the number of ultra-fine grains with high-angle boundaries increases. According to Hall–Petch relation, Eq. (2), creating new borders in ultrafine grain structures increases the strength. The effect of shear strain created during ARB process on roller friction, sample and reinforcement particles increases equivalent strain and strength [34].

$$\sigma_y = \sigma_0 + K_y d^{-1/2} \tag{2}$$

where σ_0 is the original strength of material (MPa), K_y is a constant (MPa$\sqrt{\text{m}}$) depending on material and d is the grain size of material. Also, the presence of ZrO_2

work hardening in the first cycles has the main role in increasing the strength. In addition, the formation of sub-boundaries and dislocation cells also affect the strength.

nanoparticles in aluminum matrix increases dislocation density and improves nanocomposite strength. These particles increases the strength by both partially pinning the dislocations and impeding their motion or by retarding the dislocation annihilation during deformation. So, this phenomenon increases work hardening and strength [35]. In addition, during ARB process, local strain increases around the reinforcement nanoparticles, leading to increasing the strength ratio. It has to be noted that the reinforcement nanoparticles act as a barrier to dislocation movement during the tensile test and so cause the enhancement of strength.

According to Figs. 3 and 4, it is clear that with increasing the ZrO_2 content in the aluminum matrix, the tensile strength of nanocomposites increases. When the ZrO_2 content increases, total area of the matrix/reinforcement interfaces of the nanocomposite increases too. The higher content of reinforcement leads to a higher local dislocation density or a refined grain size. Therefore, it can be concluded that with increasing the ZrO_2 content, the tensile strength of samples increases too.

Figure 5 shows the elongation value as a function of ARB cycles for the composite specimens. As seen, the elongation significantly decreases from 43 % (for annealed sample) to 10.1 % (for Al/0.5 vol % ZrO_2) and 8.4 % (for Al/0.75 vol % ZrO_2) and 7.2 % (for Al/1.0 vol % ZrO_2) by one cycle of ARB process, registering 76 and 80 and 83 % decrease, respectively. This outstanding decrease in the first step is attributed to both strain hardening mechanism and formation of two weak longitudinal interfaces between the Al layers. In fact, when the hard ZrO_2 nanoparticles are added into the matrix, the dislocations movement is hindered as a result. Therefore, the elongation value to fracture is reduced. Also, the presence of large number of Al/ZrO_2 interfaces in the nanocomposite results in significant decrease in elongation. In fact, debonding in the interfaces play an important role in decreasing the ductility. On the other hand, it is obvious that the elongation improves,
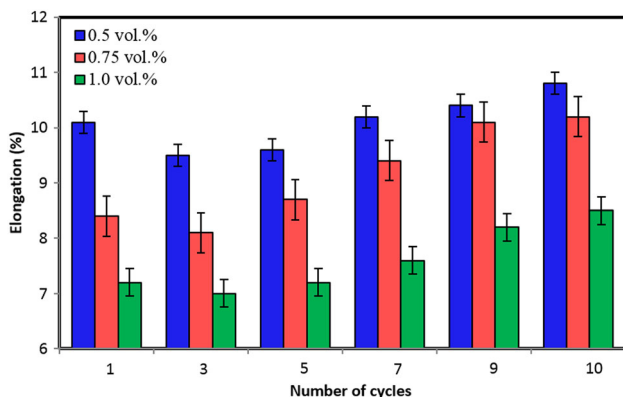
when the number of ARB cycles increases. Finally, after the 10 cycles ARB process elongation follows an incremental trend and reaches about 10.8 and 10.2 and 8.6 % for the specimen with 0.5, 0.75 and 1.0 vol% of particles, respectively. One of the factors that affect the tensile strength and elongation in the samples is proper connection of sheets in the presence of reinforcing particles and proper reinforcing particle distribution, as well as the decreased porosity [34]. The presence of porosity is a very important effect on the mechanical properties of the composite sample. In fact, the presence of porosity, especially in the vicinity of the reinforcing particles causes a sharp reduction in tensile strength and elongation [36]. There are two types of porosity in the samples produced by the ARB process which are porosity by the lack of proper connection between the sheets and porosity due to the lack of initial reinforcing particle adhesion to matrix [37].

When the number of cycles of ARB process increases, the porosity of the samples continuously decreases because of the good ductility of the pure aluminum matrix and the rolling pressure, which increases the tensile strength and elongation of Al/ZrO_2 sample composites [37]. On the other hands, when the number of ARB cycles increases and nanoparticles are no longer added to the aluminum matrix, agglomerations are eliminated and reinforcement particles distribution is improved. Nevertheless, during deformation process, the matrix-reinforcement interface is a good place for crack initiation and propagation. When the distribution of ZrO_2 particles in the Al matrix changes to be more uniform and homogeneous, the distance between the Al/ZrO_2 interfaces increases. Therefore, during plastic deformation, the cracks which are initiated in the interfaces propagates and link up with other cracks later, and the ductility of nanocomposite improves [35–39]. According to microstructural observations section, since the uniformity of particles improves due to increase in the number of ARB cycles, it can be concluded that with increasing the number of ARB cycles, the elongation of nanocomposite improves.

Figure 6 shows SEM micrograph of the fracture surface of Al/ZrO_2 nanocomposite with 1.0 vol% of particles produced by ARB process after tensile test. Fracture surface in the first cycle is in the form of ductile fracture with deep holes in the direction of stretching with matrix, having a gray surface with holes almost similar to spheroid [31]. It should be noted that fracture is first caused by micro void formation and then micro cracks join and cause emissions and ultimately create shear failures in angles related to the tension [40]. Figure 6a shows a fracture surface of a composite specimen produced by 1 vol% of particles in the first cycle with deep and stretched pores. As ARB cycles increases, fracture will change to shear mode and the number, size, depth and direction of the pores will change as well [41]. Figure 6b shows the composite

Fig. 5 Image of elongation-number of cycles for produced composites by ARB process
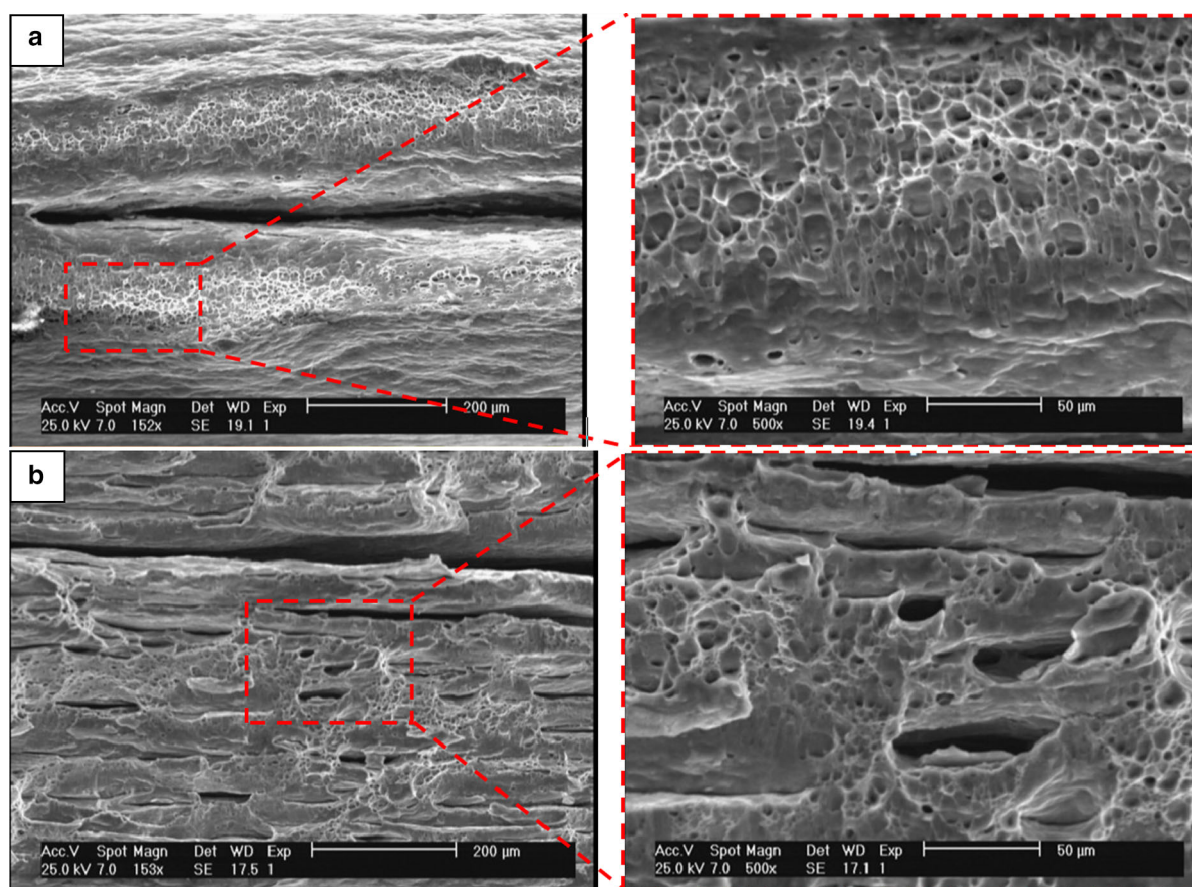
Fig. 6 The fracture surfaces of Nano-composites in **a** the first cycle and, **b** the end cycle, respectively

specimen produced by 1 vol% of particle in the final cycle (cycle 10). As can be seen in this figure the number, size, depth and direction of the pores are very different compared to the initial state (first cycle).

5 Conclusion

Al/Nano-ZrO$_2$ composites manufactured through 10 cycles of cold roll-bonding process, which was an attempt to use pure metal particle-reinforced AMMCs. The microstructure and mechanical properties of the composites were investigated. The conclusions could be summarized as follows:

1. Proper distribution of ZrO$_2$ reinforcing particles in aluminum was obtained after 10 cycles of ARB process.
2. The strength of the composite increased during ARB process. The strength of the specimen with 1 vol% ZrO$_2$ reached to 191.5 MPa which was 2.15 times higher than non-ARB aluminum sheet.
3. Elongation of the composite decreased in the first cycles and then increased as the ARB process progressed. Finally, the elongation for in 0.5, 0.75 and 1.0 vol% obtained 10.8, 10.2 and 8.6 %, respectively.

4. XRD analysis results for the specimens showed that the crystallite size after 10 cycles of ARB process in the specimen with 0.5, 0.75 and 1.0 vol% ZrO$_2$ was 85.5, 55.7 and 48.6 nm, respectively.
5. SEM images observations from the fracture surface showed that after 10 cycles of ARB process the fracture was almost shear fracture mode with fine and stretched pores.

References

1. Tsuji N, Saito Y, Lee S, Minamino Y, *Adv Eng Mater* **5** (2003) 338.
2. Lee S H, Saito Y, Tsuji N, Utsunomiya H, Sakai T. *Scr Mater* **46** (2002) 281.
3. Valiev R Z, Islamgaliev R K, Alexandrov I V, *Prog Mater Sci* **45** (2000) 103.
4. G. Sakai, Z. Horita, T.G. Langdon, Mater. Sci. Eng. A 393 (2005) 344.
5. Yin J, Lu J, Ma H, Zhang P, *J Mater Sci* **39** (2004) 2851.
6. Wang Q, Chen Y, Liu M, Lin J, Roven H J, *Mater Sci Eng A* **527** (2010) 2265.
7. Jafarian H, Borhani E, Shibata A, Terada D, Tsuji N, *J Mater Sci* **46** (2011) 4216.

8. Baazamat S, Tajally M, Borhani E, *J Alloys Compd*, **653** (2015) 39-46.
9. Hajizadeh K, Tajally M, Emadoddin E, Borhani E, *J Alloys Compd*, **588** (2014) 690.
10. Jafarian H, Borhani E, Shibata A, Tsuji N, *J Alloys Compd*, **577** (2013) 668.
11. Jafarian H, Borhani E, Shibata A, Terada D, Tsuji N, *Mater Sci Forum*, **667** (2010) 361.
12. Borhani E, Jafarian H, Adachi H, Terada D, Tsuji N, *Mater Sci Forum*, **667** (2010) 211.
13. Borhani E, Jafarian H, Shibata A, Tsuji N, *Mater Trans* **53** (2012) 1863.
14. Borhani E, Jafarian H, Terada D, Adachi H, Tsuji N, *Mater Trans* **53** (2012) 72.
15. Shu K M, Tu G C, *Mater Manuf Process* **16** (2001) 483.
16. Liu Y M, Li H C, Liou S S, Shie M T, *Master Sci Eng A* **373** (2007) 363.
17. Hosseini S A, Manesh H D, *Mater Des* **30** (2009) 2911.
18. Jamaati R, Amirkhanlou S, Toroghinejad M R, Niroumand B, *Mater Sci Eng A* **528** (2011) 2143.
19. Jamaati R, Toroghinejad M R, *Mater Sci Eng A* **527** (2010) 4858.
20. Yazdani A, Salahinejad E, *Mater Des* **32** (2011) 3137.
21. Soltani M A, Jamaati R, Toroghinejad M R, *Mater Sci Eng A* **550** (2012) 367.
22. Amirkhanlou S, Ketabchia M, Parvin N, Khorsand S, Bahrami R, *Mater Des* **51** (2013) 367.
23. Salimi S, Izadi H, Gerlich A P, *J Mater Sci* **46** (2011) 409.
24. Khorramie S A, Baghchesara M A, Lotfi R, Moradi Dehagi S, *Int J Nano Dim* **4** (2012) 261.
25. Li G, Li W, Zhang M, Tao K, *Catal Today* **93** (2004) 595.
26. Kitazono K, Kikuchi Y, Sato E, Kuribayashi K, *Mater Lett* **61** (2007) 1771.
27. Jamaati R, Toroghinejad M R, *Mater Sci Eng A* **527** (2010) 4146.
28. Akbari-Beni H, Alizadeh M, Ghaffari M, Amini R, *Compos Part B* **58** (2014) 438.
29. Kitahara H, Yada T, Tsushidab M, Andoa S, *Pro Eng* **10** (2011) 2737.
30. Monzen R, Takagawa Y, Watanabe C, Terada D, Tsuji N, *Proc Eng* **10** (2011) 2417.
31. Williamson G K, Hall W H, *Acta Metall* **1** (1953) 22.
32. Nasiri Dehsorkhi R, Qods F, Tajally M, *Mater Sci Eng A* **549** (2012) 206.
33. Borhani E, *Microstructure and Mechanical Property of Heavily Deformed Al-Sc Alloy Having Different Starting Microstructures*, PhD thesis (2012).
34. Borhani E, Jafarian H R, *J Ultrafine Grained Nanostruct Mater* **47**, (2014) 1.
35. [35] Alizadeh M, Paydar M H, *J Alloys Compds* **492** (2010) 231.
36. Jamaati R, Toroghinejad M R, Edris H, *Mater Des* **54** (2014) 168.
37. Jamaati R, Toroghinejad M R, Edris H, Salmani M R, *Mater Des* **56** (2014) 359.
38. Liu C Y, Wang Q, Jia Y Z, Zhang B, Jing R, Ma M Z, Jing Q, Liu R P, *Mater Sci Eng A* **547** (2012) 120.
39. Alizadeh M, Samiei M, *Mater Des* **56** (2014) 680-4.
40. Eizadjou M, Danesh Manesh H, Janghorban K, *J Alloys Compd* **474** (2009) 406.
41. Liu C Y, Wang Q, Jia Y Z, Zhang B, Jing R, Ma M Z, Jing Q, Liu R P, *Mater Des* **43** (2013) 367.